Northumbria
University
NEWCASTLE

Fast response/recovery H_2S gas sensor with ppb level detection limit based on α-Fe_2O_3 nanoparticles

Zhijie Li [a,*], Yanwu Huang [a], Shouchao Zhang [a], Weimei Chen [a], Zhong Kuang [a], Dongyi Ao [a], Wei Liu [a], Yong Qing Fu [b]

[a] School of Physical Electronics, University of Electronic Science and Technology of China, Chengdu, 610054, P. R. China

[b] Department of Physics and Electrical Engineering, Faculty of Engineering and Environment, Northumbria University, Newcastle Upon Tyne NE1 8ST, England

***** Corresponding author. Tel.: +86 18086810509. E-mail address: zhijieli@uestc.edu.cn (Z.-J. Li)

Abstract

H_2S gas sensor based on α-Fe_2O_3 nanoparticles was fabricated by post-thermal annealing of Fe_3O_4 precursor which was synthesized using a facile hydrothermal route. Chemical composition and microstructure of the obtained α-Fe_2O_3 nanoparticle samples were characterized. Gas-sensing performance of the sensor was investigated at different operating temperatures from 100 ^oC to 400 ^oC. Results showed that the sensor exhibited the best sensitivity, reproducibility and long-term stability for detecting H_2S gas at an operation temperature of 300 ^oC. The detection limit towards H_2S gas was 0.05 ppm, and the response time and recovery time was 30 s and 5 s, respectively. In addition, sensing mechanism of the sensor towards H_2S was discussed.

Keywords: α-Fe_2O_3; Nanoparticles; Hydrothermal; H_2S; Gas sensor

Comment [A1]: No need to include XRD, SEM, TEM here.

1. Introduction

With the development of modern industry and the improvement of people's living standards, various environmental pollution problems, such as air, water, soil and noise pollutions etc., become increasingly serious. Among these problems, air pollution has been considered as the most direct and severe one. Hydrogen sulfide (H_2S) as one of the major air pollutants, is widely found in the industrial processes including oil and natural gas drilling and refining, sewage treatment, paper milling, and is harmful to human health and environment due to its high toxicity [1, 2]. According to the safety standards established by American Conference of Government Industrial Hygienists, the threshold value defined for the H_2S is 10 ppm. Once its concentration is over 10 ppm, the human nose becomes desensitized and thus the ability to sense the H_2S declines, which may cause tragic consequence, even result in human death if the concentration is over 700 ppm [3, 4]. Therefore, developing a H_2S gas sensor with high-efficiency, low detection limit, and quick response in real-time monitoring the H_2S concentration of the surrounding environment is urgent and significant.

Currently, there are a variety of gas sensors which have been developed to detect H_2S gas, such as electrolyte solutions based electrochemical sensors, catalytic combustion based sensors and optical gas sensors [5-8]. However, these sensors suffered from a series of inherent drawbacks. For example, electrochemical sensors are applied to detect gases with active electrochemical properties and its electrodes are easily poisoned; catalytic combustion based sensors suffered from limitations on

detecting combustion gases; whereas optical sensors have problems of high manufacturing costs, poor stability and compatibility [9]. On the contrary, metal oxide semiconductor (MOS) based gas sensors possess numerous merits including low manufacturing cost, simple synthesis process, low detection limits (< ppm level) and ease of incorporation into microelectronic devices with possible high device integration density. In addition, most MOS based gas sensors tend to be long-lasted and potentially resistant to poisoning. For these reasons, they have been widely investigated. Especially, with the recent development of nanoscience and nanotechnology, a large number of nanostructured metal oxide semiconductors were developed for gas sensing application, such as In_2O_3 [10], ZnO [11, 12], WO_3 [13], α-Fe_2O_3 [14], SnO_2 [15], CuO [16] etc. Among these available types, α-Fe_2O_3 has received much research attention due to its high resistance to corrosion, abundant raw material and non-toxicity.

Hematite (α-Fe_2O_3), an n-type metal oxide semiconductor materials with a direct band gap (E_g) of 2.1 eV, is the most thermodynamically stable phase among all iron oxides under ambient conditions, and thus has been extensively used for catalysts, wastewater treatment, pigment, magnetic material, electrode materials in lithium ion batteries and gas sensor [17-22]. Particularly, for gas sensor application, it has been considered as one of the most promising sensing materials due to its high mobility of conduction electrons, good chemical and thermal stabilities. Up to now, various types of α-Fe_2O_3 with different morphologies, such as 1D nanowires and nanofibers, 2D nanobelts and nanosheets, 3D nanospheres and nanocubes [23-27], have been

successfully prepared through various routes. For gas sensing application, it is of great importance to realize a fast response and a low detection limit, but to the best of our knowledge, previously reported pure α-Fe_2O_3 based H_2S gas sensors have never achieve these properties..

In this study, we report a H_2S gas sensor based on α-Fe_2O_3 nanoparticles, which possess fast response/recovery speeds and a detection limit in ppb level. Nanoparticles of α-Fe_2O_3 were prepared using a two-step synthesis strategy including (1) preparation of Fe_3O_4 precursor through a simple hydrothermal route and (2) thermal conversion of the Fe_3O_4 precursor into α-Fe_2O_3 through post-annealing. Besides, gas sensing mechanism of the α-Fe_2O_3 gas sensor was studied.

2. Experimental procedures

2.1 Materials

Ferric nitrate ($Fe(NO_3)_3 \cdot 9H_2O$), ethanolamine ($HO(CH_2)_2NH_2$), and glucose ($C_6H_{12}O_6$) were of analytical grade , which were purchased from Sinopharm Chemical Reagents Co., Ltd (Shanghai, china) and used as received without further purification. Distilled water with a resistivity of 18.0 MΩ·cm was used throughout the synthesis process.

2.2 Synthesis

The α-Fe_2O_3 nanoparticles were synthesized using a hydrothermal reaction and then calcination treatment. In a typical synthesis process, 2.424 g ferric nitrate ($Fe(NO_3)_3 \cdot 9H_2O$) and 1.188 g glucose ($C_6H_{12}O_6$) were dissolved in 120 mL distilled water under mechanical stirring at room temperature to form a homogeneous solution. Subsequently, 2 ml ethanolamine ($HO(CH_2)_2NH_2$) was dropped into the above solution, and the solution was continually stirred for about 1 hour until the color of the mixture solution was turned into sepia. Then, the obtained homogeneous solution was transferred into a 150 mL Teflon-lined stainless steel autoclave and kept at 150 ^oC for 12 hrs. Subsequently, the autoclave was cooled down to room temperature naturally, and the resultant black precipitate was carefully collected and washed centrifugally with distilled water and absolute ethanol three times, respectively, before being dried at 80 ^oC in air for 1 hour. Finally, the reddish-brown α-Fe_2O_3 was obtained via annealing the black Fe_3O_4 precursor at 600 ^oC for 2 hrs in air.

2.3 Characterization

Crystalline structure and phase composition both Fe_3O_4 precursor and α-Fe_2O_3 were characterized by X-ray diffractometer (XRD, Rigaku D/max-2500) with Cu Kα radiation at a wavelength of 1.5406 Å operated at 40 kV and 30 mA. The morphologies of the as-prepared α-Fe_2O_3 were observed using a scanning electron microscope (SEM, Inspect F50, USA) with the operation voltage of 5 kV. Transmission electron microscope (TEM, JEM-2200FS, Japan) was used to characterized the crystallographic features of the as-prepared sample.

2.4 Gas sensor fabrication and measurements

Gas-sensing performance of the device was evaluated using a WS-30A gas sensor measurement system (Weisen Electronic Technology Co., Ltd, Zhengzhou, China). The fabrication process of the gas sensor can be described as follows: (i) the as-prepared α-Fe_2O_3 powder was mixed with the absolute ethyl alcohol with a weight ratio of 4:1 and the mixture solution was ultrasonically agitated for 15 min until a homogeneous slurry was formed; (ii) the slurry was pasted onto an alumina tube with a pair of Au electrodes and four Pt wires for resistance measurements; (iii) the alumina tube was annealed at 300 ^oC for 2 hrs to improve the stability of the sensor and remove the residual organics on the surface of sensors. Fig. 1a shows the schematic of the gas sensor, in which a Ni-Cr heater was placed inside of the alumina tube as a resistor to adjust the working temperature of the sensor. Fig.1b displays the measuring circuit of the gas sensor, where, R_E is a load resistor connected in series with the gas sensor, and R_S donates a resistor of the sensor. In the sensing test process, an appropriate bias voltage (V_S = 5 V) was applied, and through varying the heating

voltage ($V_{heating}$), different operating temperatures were obtained. The response of the sensor was measured by monitoring the voltage changes of R_E. The gas response (S) was defined as follows: $S = R_a/R_g$ for reducing gases, and $S = R_g/R_a$ for oxidizing gases, in which R_g and R_a are the resistance data of the sensor measured in the target gas and in air, respectively.

3. Results and discussion

3.1 Structural and morphological characteristics

Fig. 2a shows the XRD pattern of the as-prepared precursor, in which all the XRD peaks can be indexed to cubic phase of Fe_3O_4 (JCPDS NO.65-3107) with lattice constants of a = b = c = 8.3905 Å, Fig. 2b displays the XRD pattern of final product by annealing the precursor, and all the diffraction peaks can be indexed to those of standard hexagonal hematite (α-Fe_2O_3) (JCPDS NO.33-0664) with the lattice parameters of a = b = 5.0356 Å, c = 13.7489 Å and α = β = 90°, γ = 120°. No characteristic peaks from other Fe-related phases were observed, such as β-Fe_2O_3, γ-Fe_2O_3 etc., indicating that the Fe_3O_4 precursor was completely transferred into α-Fe_2O_3. In addition, the average crystallite sizes of the Fe_3O_4 precursor and α-Fe_2O_3 were determined to be 22 nm and 54 nm, respectively, using the Scherrer equation:

$$D = \frac{K\lambda}{B\cos\theta} \quad (1)$$

where K is scherrer constant with a value of 0.89, B is full width at half maximum (FWHM) of the diffraction peak, θ is the diffraction angle, λ is the wavelength of X-ray and D denotes the crystal size.

Fig. 3a and Fig. 3b show the SEM images of Fe_3O_4 precursor and α-Fe_2O_3. It can be seen that the Fe_3O_4 precursor composed of numerous irregular and unevenly distributed large particles, which are aggregated by a great number of small particles with an average size of 22 nm. However, from Fig. 3b, it can be observed that the as-obtained α-Fe_2O_3 film is consisted of numerous uniformly dispersed nanoparticles with an average size of about 50 nm. This difference can be attributed to the fact that

the annealing process provides the sufficient energy for mobility of the particles to realize recrystallization and grain growth [28].

To gain further insights into the crystallographic features of the as-prepared α-Fe_2O_3, TEM was employed. Fig. 4a shows a TEM image of the as-prepared α-Fe_2O_3. Obviously, the α-Fe_2O_3 was composed by numerous nanoparticles with regular shapes, and the majority particles have sizes between 35 nm and 100 nm, which are similar with those from SEM analysis. Fig. 4b shows the HRTEM image recorded on one single α-Fe_2O_3 nanoparticle, in which, a series of clear and continuous lattice fringes can be seen in the image. The typical spacing of the lattice fringes are determined to be 0.167 nm and 0.216 nm, which are corresponding to the d-spacing of the (1 1 6) and (1 1 3) planes of hexagonal α-Fe_2O_3, respectively.

3.2 Gas sensing properties and discussion

Fig. 5 shows the current-voltage characteristic curves between the two neighboring electrodes bridged by the α-Fe_2O_3 film at different working temperatures from 150 ^oC to 350 ^oC in air. It can be seen that all the currents are increased linearly with the applied bias voltage (-9 V ~ 9 V). Such a linear behavior reveals the good ohmic contacts established between the α-Fe_2O_3 film and electrodes. Moreover, with the increase of the working temperature, the conductance (S = I/V) of the α-Fe_2O_3 film was increased accordingly, which is in a good agreement with the conduction characteristics of the semiconductor.

It is well known that the operating temperature has a significant effect on the gas-sensing performance of the sensor. Thus, in order to find the optimum operating

temperature of the sensor, the response of the sensor based on α-Fe_2O_3 towards H_2S gas were measured at different working temperatures from 100 ^oC to 400 ^oC. As shown in Fig. 6, the sensing responses towards H_2S gas increased with the increased operating temperatures from 100 ^oC to 200 ^oC, and reached a maximum value at 200 ^oC, then decreased with a further increase of temperatures from 200 ^oC to 400 ^oC. This phenomenon can be explained from two aspects: (1) the kinetic of the reaction between the target gas and surface absorbed oxygen; (2) the kinetic of gas diffusion through the sensing layer [29, 30]. When the sensor operated at a low temperature, the H_2S molecules don't have enough thermal energy to react with the surface absorbed oxygen species (T<100 ^oC in this work). Therefore, the sensitivity was too low. The increase in sensitivity for the operating temperatures ranging from 100 ^oC to 200 ^oC can be attributed to the fact that the obtained thermal energy was high enough to overcome the activation energy barrier for the surface reaction. Consequently, the electron concentration increased significantly due to the enhanced surface reactions between H_2S molecules and absorbed oxygen species as shown in Eq (2).

$$2H_2S + 6O^- \rightarrow 2H_2O + 2SO_2 + 6e^- \quad (2)$$

However, when the operating temperature is above 200 ^oC, the sensitivity decreased, which can be attributed to the utilization rate of the sensing layer was decreased, because the target gas (H_2S) was just consumed at a very shoallow surface of the sensing layer in this case, which leads to the reduction of the diffusion depth of the target gas, therefore, the change in the resistance would be decreased. Consequently, the sensitivity is decreased [29].

The response and recovery time, which are linked closely with the detection speed of the sensor, are two important parameters in evaluating the gas-sensing performance of the sensors. Here, the response time and recovery time were defined as the time to reach 90% of the maximum sensing response when the target gases was injected into the chamber, as well as the time for the maximum sensing response was decrease to 10% upon air purging. Fig. 7 shows the response time and recovery time of the sensor based on α-Fe_2O_3 nanoparticles upon exposure to 10 ppm H_2S gas at operating temperatures from 100 ^oC to 400 ^oC. It can be observed obviously that a higher operating temperature is beneficial to the decrease of the response and recovery time. This phenomenon can be explained as follow: (1) the adsorption and desorption processes are thermally reactions, which are sensitive to the temperature; (2) the increased working temperature will accelerate the electron transition between the conductor band and surface Fermi level, which could facilitate the desorption reaction, thus, the recovery time is greatly decreased. In this study, when the operating temperature was higher than 300 ^oC, the response time and recovery time of the sensor were 30 s and 5 s, respectively.

Considering the sensitivity and response-recovery time of the sensors operating at different temperatures, we have chosen 300 ^oC as the optimum temperature to further investigate the sensing performance of the α-Fe_2O_3 nanoparticle based sensor. Fig. 8 displays the real-time gas sensing transients of the sensor to 10 ppm H_2S gas at 300 ^oC. The almost square shape response observed in the curve indicates that the sensor has a rapid response to H_2S gas and achieves a steady state in a short time. The resistance

undergoed a dramatic decrease upon the injection of H_2S gas and almost recovered to its initial value when the H_2S flow was switched off, indicating a good reversibility the sensor possesses. In addition, the response time and recovery time were determined to be 30 s and 5 s, respectively.

The response and recovery behaviors of the sensor were further investigated by exposing the sensors to different concentrations of H_2S gas at the operating temperature of 300 ^oC, and the results are shown in Fig. 9. Dry air was firstly used to purge the testing chamber to obtain the baseline, and then the H_2S gas was introduced into the testing chamber. When the sensor was exposed to the H_2S gas from 10 ppm down to 0.05 ppm, the corresponding responses shown in Fig. 7a and Fig. 7b are 5.31 to 1.25, clearly indicating that the sensor has a high sensitivity down to sub-ppm level for the H_2S gas detection. Although the other oxide sensors reported in the literature could also detect H_2S at sub-ppm level, such as In_2O_3 [10], WO_3 [13], CuO [31-33] etc., their response/recovery durations were quite long. For example, Ramgir et al reported that the detection limit of the CuO-SnO_2 thin film based senor to H_2S gas was as low as 0.02 ppm at the operating temperature of 300 ^oC. However, the response time and recovery time of that sensor were 20 min and 10 min, respectively, much longer than those from our work (30 s and 5 s). Besides, in the Fig. 9c and Fig. 9d, the response of the sensor was enhanced linearly with the increase of H_2S concentration, indicating a good linearity of the sensing characteristics.

Considering the practical application of the fabricated gas sensor, the reproducibility of the α-Fe_2O_3 based sensor was further investigated by successively

exposing the sensor to the H_2S gas at the concentration of 10 ppm for 4 cycles, and the corresponding curve of the response-recovery characteristic is shown in Fig. 10. During the successive gas injection and releasing, the response-recovery curves of the sensor are repeated without apparent changes. Fig.10 (b) shows error bars of the sensor responses by successively exposing the sensor to 10 ppm H_2S gas for four cycles. The largest standard deviation (SD) was less than 0.1, indicating that the sensor based α-Fe_2O_3 nanoparticles possesses a good reproducibility.

Long-term stability, one of the most important parameters for the sensor during the practical application, has been characterized and is shown in Fig. 11. The sensor exhibits a nearly constant response to 5 ppm and 10 ppm H_2S gas during the 16 days continuous test, suggesting the sensor possess an excellent long-term stability for H_2S detection.

3.3 Gas sensing mechanism

The H_2S sensing mechanism of α-Fe_2O_3 nanoparticles based sensor is illustrated in Fig. 12. As is well known, α-Fe_2O_3 is an n-type metal oxide semiconductor, and its sensing performance is governed by the change of the surface resistance resulted from the chemical interaction between the test gases and the oxygen species absorbed on the surface of the sensor [34, 35]. When the sensor is placed in an Ar atmosphere, the energy band is close to the flat-band situation because there is no electrons transfer between surface Fermi level and conductor band as shown in Fig. 12a [36]. However, once the α-Fe_2O_3 was exposed to the air, the oxygen molecules was absorbed on the surface of α-Fe_2O_3, and formed negatively charged chemisorbed

oxygen species (O_2^-, O^-, O^{2-}) by capturing electrons from conduction band and trapping them at the surface. This would result in a decrease in the conductivity of the sensor and the upward bending of energy band, thus producing an electron-depletion layer on the surface and generating a barrier Δφ as shown in Fig. 12b. The types of absorbed oxygen species are dependent on the working temperature. When the temperature was lower than 100 ^oC, O_2^- was commonly chemisorbed. However, when the temperature was between 100 ^oC and 300 ^oC, O^- became commonly chemisorbed and the O_2^- disappeared rapidly. Once the temperature was higher than 300 ^oC, the oxygen species mainly existed in the form of O^{2-} [37]. The absorption process on the surface can be depicted as follow:

$$O_{2(g)} \rightarrow O_{2(ad)} \quad (3)$$

$$O_{2(ad)} + e^- \rightarrow O_{2(ad)}^- \quad (T < 100\ ℃) \quad (4)$$

$$O_{2(ad)}^- + e^- \rightarrow 2O_{(ad)}^- \quad (100\ ℃ < T < 300\ ℃) \quad (5)$$

$$O_{(ad)}^- + e^- \rightarrow O_{(ad)}^{2-} \quad (T > 300\ ℃) \quad (6)$$

When the sensor was exposed to the H_2S gas, these absorbed oxygen species would react with the H_2S molecules and generate sulfur oxides and H_2O vapor. During this process, the captured electrons would be released back into the conduction band. As a result, the surface resistance of the α-Fe_2O_3 was decreased, the electron-depletion layer was reduced and the potential barrier (Δφ) was decreased. This chemical interaction can be described below:

$$2H_2S_{(g)} + 3O_{2(ad)}^{\alpha-} \leftrightarrow 2H_2O_{(g)} + 2SO_{2(g)} + 3\alpha \cdot e^- \quad (7)$$

Because the sensing material consists of connected nanoparticles, thus, the carrier

transfer between those overlapped nanoparticles was also investigated. The corresponding schematic diagram is shown in Fig. 13. When the particles are connected or contacted, a transmission path will be generated among these nanoparticles. Consequently, due to the partial concentration gradient of carriers among these connected particles, the carriers will diffuse along this transmission path. Additionally, when a bias voltage is applied, an extra electric field will be generated among these particles, thus, the carriers will drift along the opposite or positive direction of the electric field from one particle to another. Under these conditions, a contact barrier will be formed between these connected particles. Once the sensor is placed in the presence of H_2S gas, the surface reaction between the absorbed oxygen species and H_2S molecules will release electrons. In this process, some of these released electrons will return to the conductor band, and others will hop into the contact barrier area, which reduces the width of the contact barrier, resulting in the decrease of contact resistance between the overlapped particles [38, 39].

4. Conclusions

In summary, α-Fe_2O_3 nanoparticles were synthesized by a facile and eco-friendly hydrothermal reaction combined with a subsequent calcination process. The H_2S sensing properties including sensitivity, reversibility, reproducibility and stability were studied. Results showed that the optimum operating temperature to detect H_2S gas is 300 ^oC, in which, the lowest detection limit to H_2S gas reaches 0.05 ppm with the response value of 1.25, and the response and recovery time of the sensor to 10 ppm H_2S gas are as low as 30 s and 5 s, respectively. In addition, the sensor also exhibits excellent reproducibility and long-term stability for H_2S detection, indicating that the α-Fe_2O_3 nanoparticles synthesis by this method can be a promising sensing material for fabrication high-performance H_2S gas sensor.

Acknowledgments

This work was supported by the Fundamental Research Funds for the Central Universities (ZYGX2012J047), the Joint Fund of the National Natural Science Foundation of China and the China Academy of Engineering Physics (U1330108). Royal Academy of Engineering: Research Exchange between UK and China.

References

[1] D.W. Dockery, J. Schwartz, J.D. Spengler, Air pollution and daily mortality: associations with particulates and acid aerosols, Environ. Res. 59 (1992) 362–373.

[2] N. Yamazoe, Toward innovations of gas sensor technology, Sens. Actuator B: Chem. 108 (2005) 2–14.

[3] A.D. Wiheeb, I.K. Shamsudin, M.A. Ahmad, M.N. Murat, J. Kim, M.R. Othman, Present technologies for hydrogen sulfide removal from gaseous mixtures, Rev. Chem. Eng. 29 (2013) 449−470.

[4] C. Chou, Hydrogen Sulfide: Human Health Aspects: Concise International Chemical Assessment Document 53. World Health Organization, Geneva, 2003.

[5] C.B. Yu, Y.J. Wang, K.F. Hua, W. Xing, T.H. Lu, Electrochemical H_2S sensor with H_2SO_4 pre-treated Nafion membrane as solid polymer electrolyte, Sens. Actuator B: Chem. 86 (2002) 259-265.

[6] X.F. Liu, H.P. Dong, S.H. Xia, Micromachined catalytic combustion type gas sensor for hydrogen detection, Micro & Nano Lett. 8 (2013) 668-671.

[7] M.M.F. Choi, P. Hawkins, Development of an optical hydrogen sulphide sensor, Sens. Actuator B: Chem. 90 (2003) 211–215.

[8] W.W. Feng, N. Zhou, L.G. Chen, B.W. Li, An optical sensor for monitoring of dissolved oxygen based on phase detection, J. Opt. 15 (2013) 055502.

[9] S.M. Kanan, O.M. El-Kadri, I.A. Abu-Yousef, M.C. Kanan, Semiconducting Metal Oxide Based Sensors for Selective Gas Pollutant Detection, Sensors. 9 (2009) 8158-8196.

[10] K. Yao, D. Caruntu, Z.M. Zeng, J.J. Chen, C.J. O'Connor, W.L. Zhou, parts per billion-level H_2S detection at room temperature based on self-assembled In_2O_3 nanoparticles, J. Phys. Chem. C 113 (2009), 14812-14817.

[11] S.Y. Wang, J.Y. Ma, Z.J. Li, H.Q. Su, N.R. Alkurd, W.L. Zhou, L. Wang, B. Du, Y.L. Tang, D.Y. Ao, S.C. Zhang, Q.K. Yu, X.T. Zu, Surface acoustic wave ammonia sensor based on ZnO/SiO2 composite film, J. Hazard. Mater. 285 (2015) 368-374.

[12] Z.S. Hosseini, A. Mortezaali, A.I zad , S. Fardindoost, Sensitive and selective room temperature H_2S gas sensor based on Au sensitized vertical ZnO nanorods with flower-like structures, J. Alloy. Compd. 628 (2015) 222-229.

[13] Y.B. Shen, B.Q. Zhang, X.M. Cao, D.Z. Wei , J.W. Ma, L.J. Jia, S.L. Gao, B.Y. Cui, Y.C. Jin, Microstructure and enhanced H_2S sensing properties of Pt-loaded WO_3 thin films, Sens. Actuator B: Chem. 193 (2014) 273–279.

[14] Y. Wang, Y.M. Wang, J.L. Cao, F.H. Kong, H.J. Xia, J. Zhang, B.L. Zhu, S.R. Wang, S.H. Wu, Low-temperature H_2S sensors based on Ag-doped α-Fe2O3 nanoparticles, Sens. Actuator B: Chem.131 (2008) 183–189.

[15] S.M. Zhang, P.P. Zhang, Y. Wang, Y.Y. Ma, J. Zhong, X.H. Sun, Facile fabrication of well-ordered porous Cu-doped SnO_2 thin film for H_2S sensing, Appl. Mater. Inter. 6 (2014) 14975−14980.

[16] F. Teng, W. Yao, Y. Zheng, Y. Ma, Y. Teng, T. Xu, S. Liang, Y. Zhu, Synthesis of flower-like CuO nanostructures as a sensitive sensor for catalysis, Sens. Actuator B: Chem.134 (2008) 761-768.

[17] Z.J Li, W.Z Shen, W.S He, X.T Zu, Effect of Fe-doped TiO_2 nanoparticle derived from modified hydrothermal process on the photocatalytic degradation performance on methylene blue, J. Hazard. Mater 155 (2008) 590-594.

[18] L. Yue, K.H. Wang, J.B. Guo, J.L. Yang, X. Luo, J. Lian, L. Wang, Enhanced electrochemical oxidation of dye wastewater with Fe_2O_3 supported catalyst, J. Ind. Eng. Chem. 20 (2014) 725–731.

[19] H. Katsuki, S. Komarneni, Role of α-Fe_2O_3 morphology on the color of red pigment for porcelain, J. AM. Ceram. Soc. 86 (2003) 183-185.

[20] J.T. Wu, S.Y. Mao, Z.G. Ye, Z.X. Xie, L.S. Zheng, Room-temperature weak ferromagnetism induced by point defects in alpha-Fe2O3, Appl. Mater. Inter. 2 (2010) 1561-1564.

[21] M.H. Chen, J.L. Liu, D.L. Chao, J. Wang, J.H. Yin, J.Y. Lin, H.J. Fan, Z.X Shen, Porous alpha-Fe2O3 nanorods supported on carbon nanotubes-graphene foam as superior anode for lithium ion batteries, Nano. Energy. 9 (2014) 364-372.

[22] Minghua Chena, Jilei Liu, Dongliang Chao, Jin Wang, Jinghua Yin, Jianyi Lin, Hong Jin Fan, Ze Xiang Shen, Porous α-Fe2O3 nanorods supported on carbon nanotubes-graphene foam as superior anode for lithium ion batteries, Nano Energy (2014) 9, 364–372.(重复)

[23] W. Zheng, Z.Y. Li, H.N. Zhang, W. Wang, Y. Wang, C. Wang, Electrospinning route for α-Fe_2O_3 ceramic nanofibers and their gas sensing properties, Mater. Res. Bull. 6 (2009) 1432-1436.

Comment [A2]: ?? Format?

[24] Z. Sun, H. Yuan, Z. Liu, B. Han, X. Zhang, A highly efficient chemical sensor material for H_2S: α-Fe_2O_3 nanotubes fabricated using carbon nanotube templates, Adv. Mater. 17 (2005) 2993-2997.

[25] L. Liao, Z. Zheng, B. Yan, J. X. Zhang, H. Gong, J. C. Li, C. Liu, Z. X. Shen, T. Yu, Morphology Controllable Synthesis of α-Fe_2O_3 1D Nanostructures: Growth Mechanism and Nanodevice Based on Single Nanowire, J. Phys. Chem. C. 112 (2008) 10784-10788.

[26] H. Shan, C.B. Liu, L. Liu, J.B. Zhang, H.Y. Li, Z. Liu, X.B. Zhang, X.Q. Bo, X. Chi, Excellent Toluene Sensing Properties of SnO2-Fe2O3 Interconnected Nanotubes, ACS. Appl. Mater. Inter. 13 (2013) 6376-6380.

[27] J.W. Deng, J.M. Ma, L. Mei, Y.J. Tang, Y.J. Chen, T. Lv, Z. Xu, T.H. Wang, Porous α-Fe_2O_3 nanosphere-based H2S sensor with fast response, high selectivity and enhanced sensitivity, J. Mater. Chem. A. 1 (2013) 12400-12403.

[28] H. Asgharzadeh, H.J. McQueen, Grain growth and stabilisation of nanostructured aluminium at high temperatures: review, Mater. Sci. Tech. 31 (2015) 1016-1034.

[29] P. Sun, X. Zhou, C. Wang, K. Shimanoe, G.Y. Lu, N. Yamazoe, Hollow SnO2/a-Fe2O3 spheres with a double-shell structure for gas sensors, J. Mater. Chem. A 2 (2014) 1302-1308.

[30] J.F. Chang, H.H. Kuo, I.C. Leu, M.H. Hon, The effects of thickness and operation temperature on ZnO:Al thin film CO gas sensor, Sens. Actuators B 84 (2002) 258-264.

[31] J. Chen, K. Wang, L. Hartman, W. Zhou, H2S detection by vertically aligned

CuO nanowire array sensors, J. Phys. Chem. C 112 (2008) 16017-16021.

[32] J. Tamaki, K. Shimanoe, Y. Yamada, Y. Yamamoto, N. Miura, N. Yamazoe, Dilute hydrogen sulfide sensing properties of CuO-SnO2 thin film prepared by low pressure evaporation method, Sens. Actuators B 49 (1998) 121-125.

[33] N.S. Ramgir, S.K. Ganapthi, M. Kaur, N. Datta, K.P. Muthe, D.K. Aswal, S.K. Gupta, J.V. Yakhmi, Sub-ppm H_2S sensing at room temperature using CuO thin films,Sens. Actuators B 151 (2010) 90-96.

[34] J.Y. Kim, K.J. Yong, Mechanism study of ZnO nanorod-bundle sensors for H_2S gas sensing, J. Phys. Chem. C. 115 (2011) 7218-7224.

[35]Z. Wen, L.P. Zhu, Y.G. Li, Z.Y. Zhang, Z.Z. Ye, Mesoporous Co_3O_4 nanoneedle arrays for high-performance gas sensor, Sens. Actuators. B. 203 (2014) 873–879.

[36] C. Feng, S. Ruan, J. Li, B. Zou, J. Luo, W. Chen, W. Dong, F. Wu, Ethanol sensingproperties of LaCoxFe1 − xO3nanoparticles: effects of calcination temperature,co-doping, and carbon nanotube-treatment, Sens. Actuators B: Chem. 155(2011) 232–238.

[37]S.J. Chang, T.J. Hsueh, I.C Chen, B.R Huang, Highly sensitive ZnO nanowire CO sensors with the adsorption of Au nanoparticles, Nanotechnology. 19 (2008) 175502.

[38] X.J Wan, J.L Wang, L.F Zhu, J.N Tang, Gas sensing properties of Cu_2O and its particle size and morphology-dependent gas-detection sensitivity. J. Mater. Chem. A 2 (2014) 13641-13647.

[39] L. Rassaei, M. Herrmann, S.N. Gordeev, F. Marken, Inter-particle charge transfer in TiO2-phytate films: Generator-collector gold-gold junction transients, J.

Electroanal. Chem. 686 (2012) 32-37.

Figure Captions

Fig.1 (a) Schematic of the gas sensor based on α-Fe_2O_3 nanoparticles. (b) The measuring electric circuit for the gas sensor.

Fig. 2 XRD patterns of as-prepared samples: (a) the Fe_3O_4 precursor and (b) the final product of α-Fe_2O_3.

Fig. 3 SEM images of (a) the as-prepared Fe_3O_4 precursor (b) the α-Fe_2O_3 product

Fig. 4 (a) Wide-field TEM image of as-prepared α-Fe_2O_3, (b) The corresponding HRTEM image of single α-Fe_2O_3 nanoparticle.

Fig. 5 I-V characteristics curves of the sensor at different operating temperatures (150 ^oC, 200 ^oC, 250 ^oC, 300 ^oC, 350 ^oC corresponding to the curves from 1 to 5, respectively)

Fig. 6 (a) Gas response of the α-Fe_2O_3 nanoparticles based gas sensor as a function of working temperature to various concentrations H_2S gas ranging from 1 ppm to 10 ppm.

Fig. 7 Response time and recovery time of the sensor based on α-Fe_2O_3 nanoparticles upon exposure to 10 ppm H_2S gas at an operating temperature from100 ^oC to 400 ^oC.

Fig. 8 Real-time gas sensing transients of the sensor based on α-Fe_2O_3 nanoparticles to 10 ppm H_2S gas at 300 ^oC.

Fig. 9 Dynamic response-recovery curve of the α-Fe_2O_3 nanoparticles based sensor upon exposure to H_2S gas with various concentrations of: (a) 1 ppm-10 ppm, (b) 0.05 ppm-0.5ppm at the optimum working temperature of 300 ^oC. Linear plot of sensitivity as a function of the concentrations of H_2S gas: (c) 1 ppm-10 ppm, (d) 0.05 ppm-0.5 ppm.

Fig. 10 (a) Reproducibility of the sensor based on α-Fe_2O_3 nanoparticles by successively exposing the sensor to 10 ppm H_2S gas at 300 ^oC. (b) The sensitivity fluctuation range and (c) response/ recovery time fluctuation range during four successively exposure the sensor to 10 ppm H_2S at 300 ^oC.

Fig .11 long-term stability of the gas sensor based on α-Fe_2O_3 nanoparticles to 5 ppm and 10 ppm H_2S gas at 300 ^oC

Fig. 12 Band diagrams and schematic images of the surface reactions at different surroundings: (a) in the Ar atmosphere; (b) exposed in the air (c) in the presence of H_2S gas.

Fig .13 Gas sensing mechanism and carrier transfer between two overlapped particles.

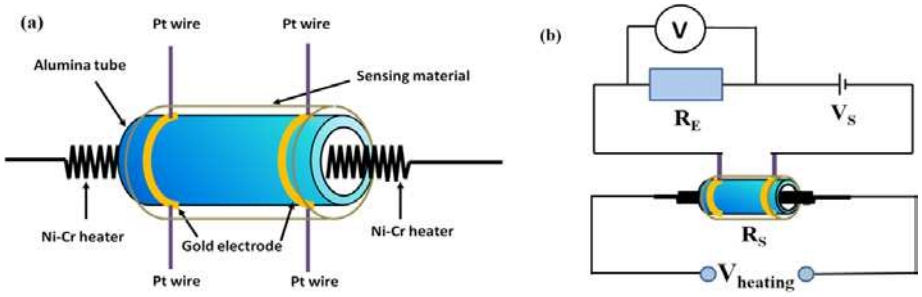

Fig.1 (a) Schematic of the gas sensor based on α-Fe_2O_3 nanoparticles. (b) The measuring electric circuit for the gas sensor

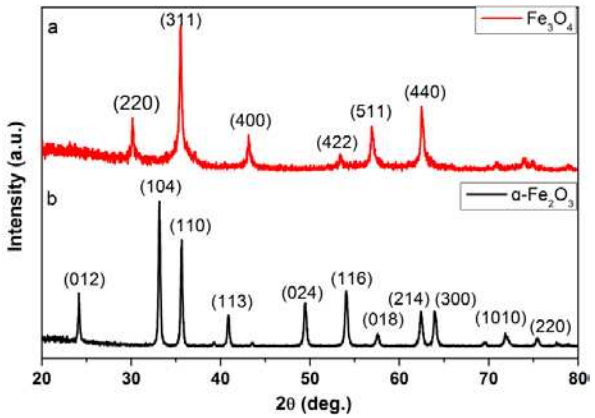

Fig. 2 XRD patterns of as-prepared samples: (a) the Fe_3O_4 precursor and (b) the final product of α-Fe_2O_3

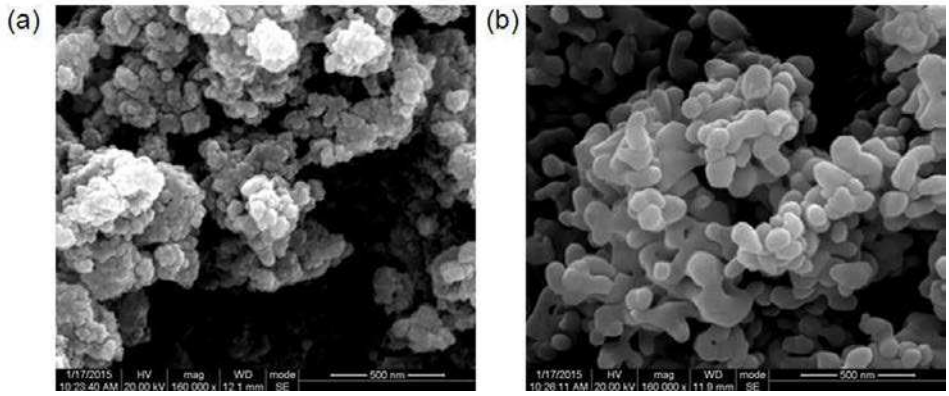

Fig. 3 SEM images of (a) the as-prepared Fe_3O_4 precursor (b) the α-Fe_2O_3 product

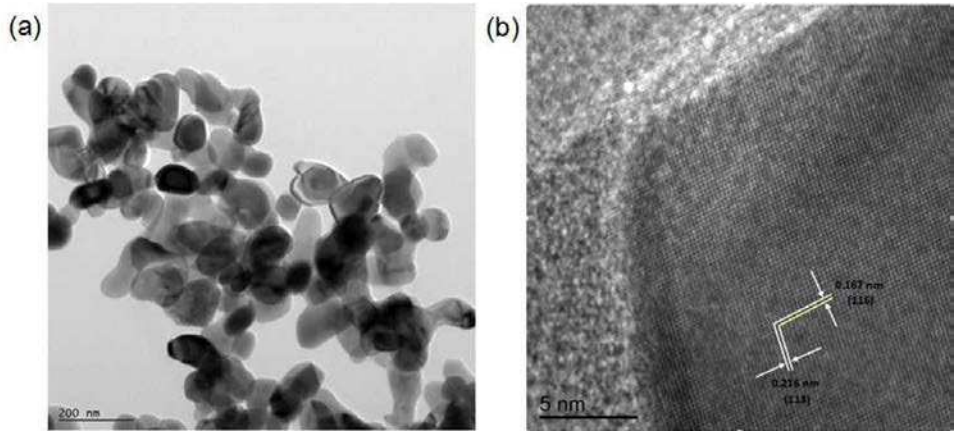

Fig. 4 (a) Wide-field TEM image of as-prepared α-Fe_2O_3, (b) The corresponding

HRTEM image of single α-Fe_2O_3 nanoparticle

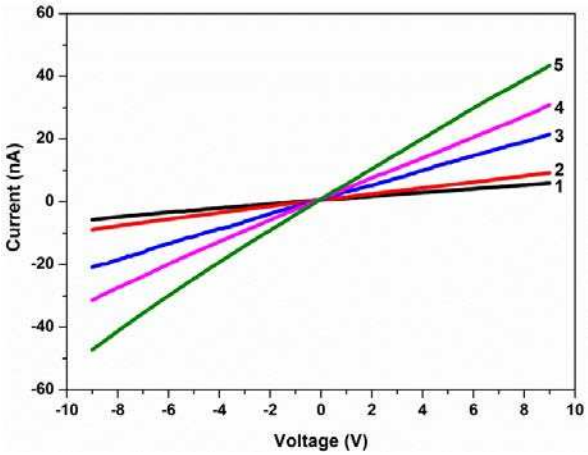

Fig. 5 I-V characteristics between the two neighboring electrodes bridged by the α-Fe_2O_3 film at different working temperature ranging from 100 ^oC to 350 ^oC

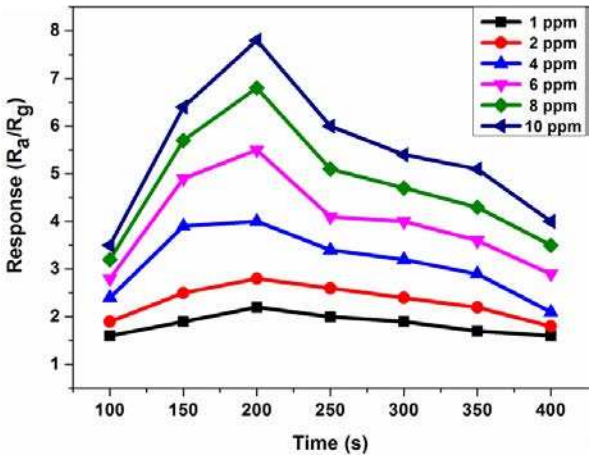

Fig. 6 (a) Gas response of the α-Fe_2O_3 based sensor to different concentrations of H_2S gas measured at different working temperature.

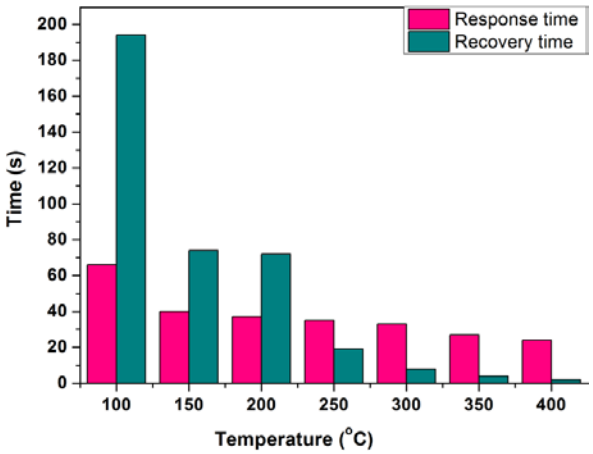

Fig. 7 Response time and recovery time of the sensor derived from α-Fe_2O_3 upon exposure to 10 ppm H_2S gas at an operating temperature in the range of 100 ^oC- 400 ^oC.

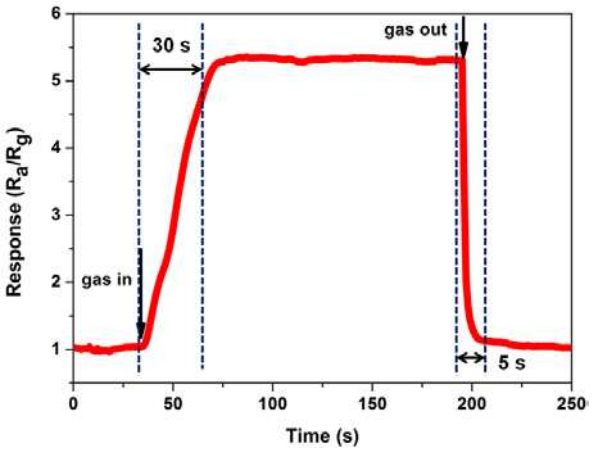

Fig. 8 Real-time gas sensing transients of the sensor based on α-Fe_2O_3 nanoparticles to 10 ppm H_2S gas at 300 ^oC.

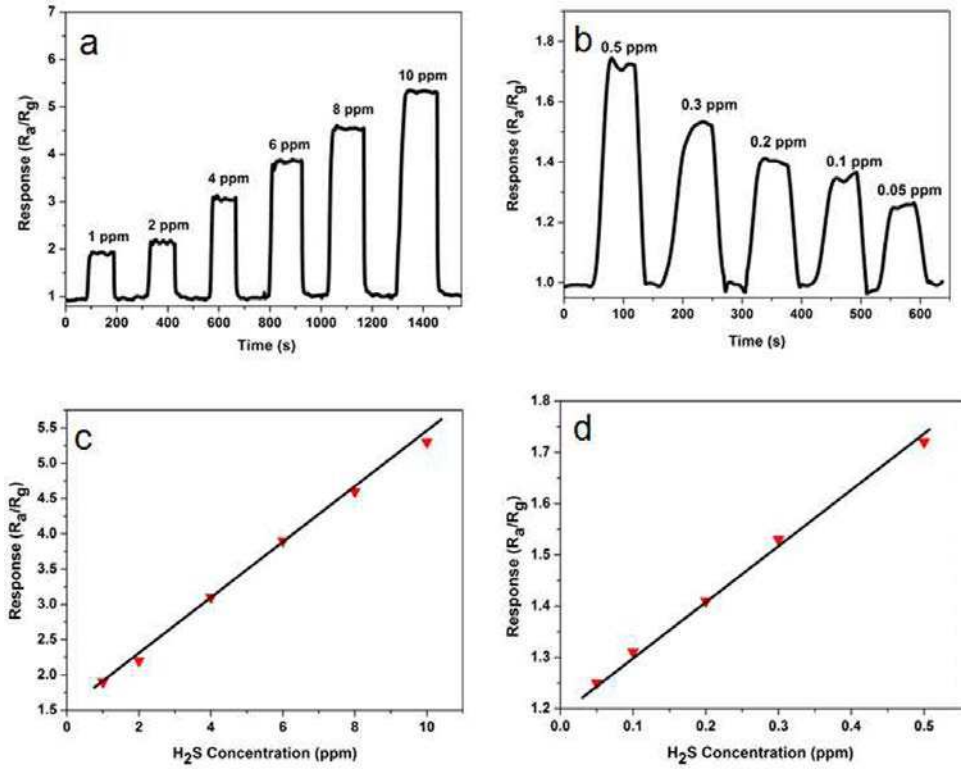

Fig. 9 Dynamic response-recovery curve of the α-Fe_2O_3 based sensor upon exposure to different concentration H_2S gas at the operating temperature of 300 ^oC: (a) 1 ppm -10 ppm, (b) 0.05 ppm-0.5ppm. Linear plot of sensitivity as a function of the concentrations of H_2S gas: (c) 1 ppm-10 ppm, (d) 0.05 ppm-0.5 ppm.

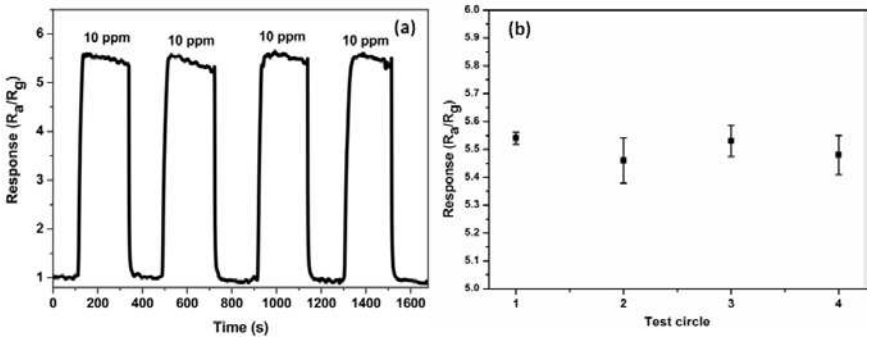

Fig. 10 (a) Reproducibility of the sensor based on α-Fe_2O_3 nanoparticles by

successively exposing the sensor to 10 ppm H_2S gas at 300 ^oC. (b) Error bar of the sensor's response by successively exposure the sensor to 10 ppm H_2S gas four circles.

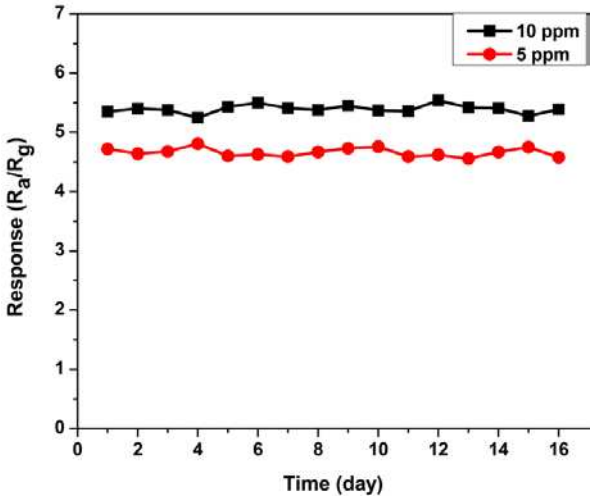

Fig .11 long-term stability of the gas sensor based on α-Fe_2O_3 nanoparticles to 5 ppm and 10 ppm H_2S gas at 300 ^oC

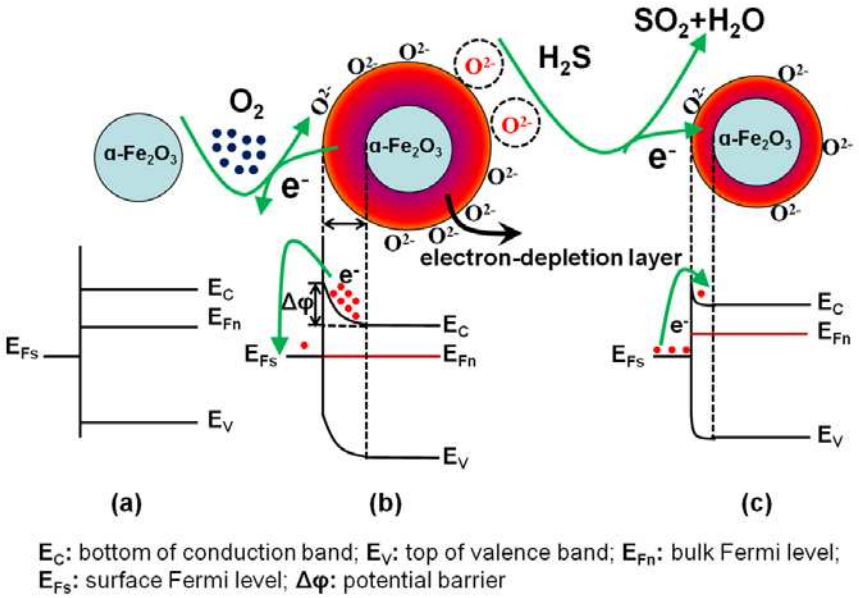

Fig. 12 Band diagrams and schematic images of the surface reactions at different

surroundings: (a) in the Ar atmosphere; (b) exposed in the air (c) in the presence of H_2S gas.